JACS
JOURNAL OF THE AMERICAN CHEMICAL SOCIETY
pubs.acs.org/JACS
Communication

Observation of Möbius Aromatic Planar Metallaborocycles

Ling Fung Cheung, G. Stephen Kocheril, Joseph Czekner, and Lai-Sheng Wang*

Cite This: J. Am. Chem. Soc. 2020, 142, 3356−3360
Read Online
ACCESS | Metrics & More | Article Recommendations | Supporting Information

ABSTRACT: Möbius aromaticity was developed for twisted annulenes with electron counting rules opposite to those of Hückel aromaticity. The introduction of transition metals makes it possible for *planar* cyclic systems to exhibit Möbius aromaticity. Here we report the first planar monocyclic metallaboron systems with Möbius aromaticity. The structures and bonding of two rhenium-boride clusters are studied by high-resolution photoelectron imaging and ab initio calculations. The ReB_3^- cluster is shown to have a near-pyramidal structure, while ReB_4^- is found to be a planar pentagonal ring. Chemical bonding analyses show that both ReB_4^- and ReB_4 possess four delocalized π-electrons, including two π-electrons in an orbital of Möbius topology. NICS calculations reveal strong aromatic characters in ReB_4^- and ReB_4, consistent with the $4n$ electron counting rule for Möbius aromaticity.

A Möbius strip can be realized by taking a paper strip, twisting it by 180°, and then joining its two ends to form a loop. Heilbronner first considered the Hückel molecular orbitals (MOs) of Möbius-type annulenes and showed that they are aromatic with $4n$ π-electrons or antiaromatic with $4n + 2\pi$-electrons.[1] The electron counting rule for Möbius aromaticity is opposite to that for Hückel aromaticity because of the *phase change* of the overlapping p_z-orbitals caused by the 180° twist in the Möbius topology. Because of the ring strain induced by the twist,[2] the first Möbius aromatic molecule synthesized, [16]annulene, was stabilized by a "belt-like" aromatic motif.[3] Craig and Paddock proposed "a novel type of aromaticity" earlier by considering $p_\pi-d_\pi-p_\pi$-interactions in cyclic molecules containing a S- or P-atom.[4] Interestingly, d-orbitals can induce a phase change in the overlapping p_z-orbitals in *planar* cyclic systems if the tangential d-orbital (d_{yz}) conjugates with the p_z-orbitals on the neighboring atoms, such as in metallabenzenes.[5] Although the bonding in metallabenezenes is complicated,[6,7] Möbius aromaticity was demonstrated computationally in planar metallacycles with $4n$ π-electrons.[8] Planar bicyclic osmapentalynes were synthesized and were shown to exhibit Möbius aromaticity.[9] Recently, Möbius aromaticity in planar metallacycles has drawn significant interest.[10−17]

The structures and bonding of size-selected boron clusters (B_n^-) have been extensively investigated using photoelectron spectroscopy (PES) and computational chemistry.[18−20] Small boron clusters have been found to be planar and aromatic following the Hückel rules.[21−28] Recently, we reported an aromatic metallaboron analogue of metallabenzenes, ReB_6^-, which was found to possess a planar hexagonal structure with a central B-atom and six delocalized π-electrons.[29] An interesting question arises: can Möbius aromatic metallaboron clusters exist? Transition-metal-doped boron clusters have been investigated by PES and computational chemistry.[30−33] Larger MB_n^- clusters form aromatic metal-centered molecular wheels, such as $Re©B_8^-$ and $Re©B_9^-$ or half-sandwich structures.[34,35] Hence, we focus our efforts on smaller transition-metal-doped boron clusters to search for Möbius aromaticity. Here we report the first observation of a Möbius aromatic metallaboron in ReB_4^-, which has a planar pentagonal structure with four π-electrons. Its Möbius aromaticity is confirmed by calculations using the nuclear-independent chemical shift (NICS).[36]

The experiments were conducted using a high-resolution PE-imaging apparatus, which has been described previously (see SI for more details).[37] The PE images and spectra of ReB_3^- at four photon energies are shown in Figure 1. The full data set at 10 photon energies is given in Figure S1. The first peak (X) denotes the 0−0 transition and the electron affinity (EA) of ReB_3. The spacing between peaks X, a, d, h, and n are similar, indicating that they belong to the same vibrational progression. Similarly, peaks b, g, and q correspond to the same vibrational progression. The strong Franck−Condon activities in the PE spectra indicate that ReB_3^- undergoes a large geometric change upon photodetachment. The measured binding energies of each peak and their vibrational assignments are given in Table S1. The vibrational assignments of the most active modes are shown in Figure S2.

The PE images and spectra of ReB_4^- (Figure 2) display a sharp and intense 0−0 peak (X) followed by weak vibrational peaks. This observation suggests that there is a small structure change between the ground states of ReB_4^- and ReB_4. The binding energies of the observed peaks, their energy shifts relative to peak X, and assignments are summarized in Table S2.

We performed theoretical calculations to search for the global minima of ReB_3^- and ReB_4^- (see SI for details).[38,39] ReB_3^- was found to have a near-pyramidal structure (Figure 3a). A planar structure was found to be 0.45 eV higher in energy (Figure S3a). The global minimum of neutral ReB_3 was

Received: December 12, 2019
Published: February 10, 2020

https://dx.doi.org/10.1021/jacs.9b13417
J. Am. Chem. Soc. 2020, 142, 3356−3360

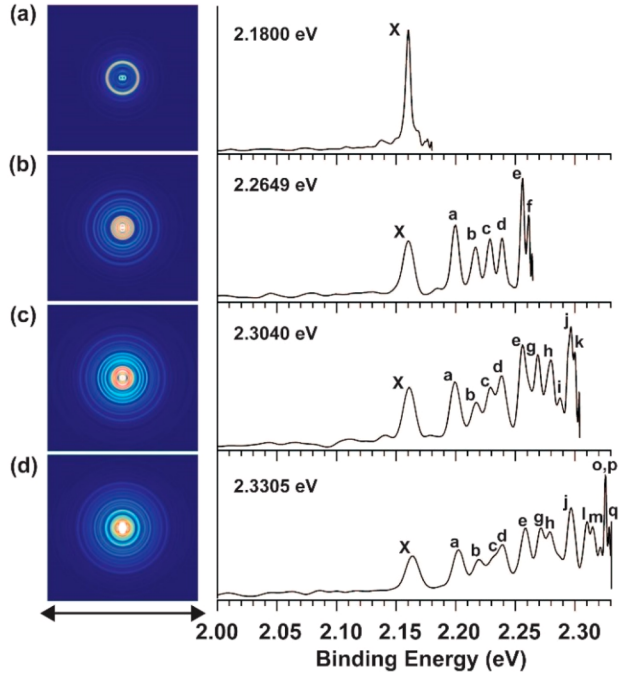

Figure 1. Photoelectron images and spectra of ReB_3^- at four photon energies. The double arrows denote the laser polarization.

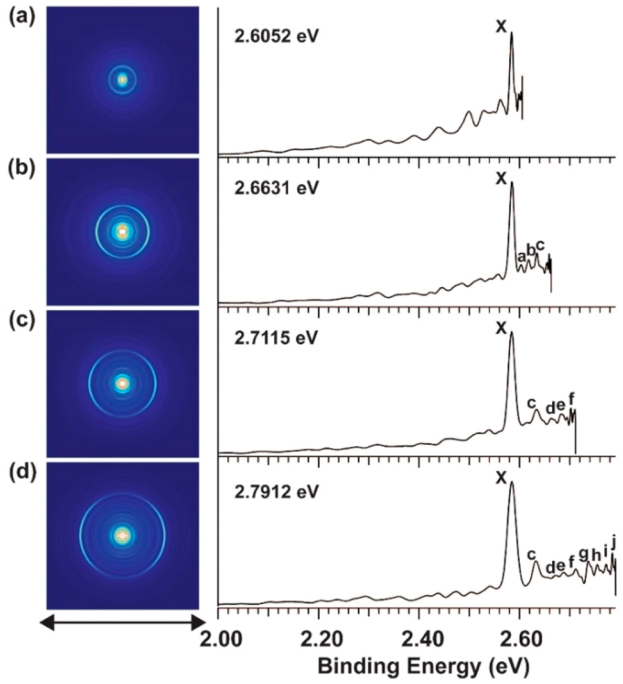

Figure 2. Photoelectron images and spectra of ReB_4^- at four photon energies. The double arrows denote the laser polarization.

also found to be near-pyramidal (Figure 3b), with a triplet pyramidal structure being 0.12 eV higher in energy and a triplet planar structure being 0.27 eV higher in energy (Figure S3b). We found that the global minimum of ReB_4^- (Figure 3c) has a planar pentagonal ring structure; a triplet state is 0.33 eV higher in energy (Figure S3c). The ground state of ReB_4 is a spin doublet with almost the same structure as that of the anion (Figure 3d).

There are large differences in the calculated bond lengths between the boron atoms in the ground state of ReB_3^- (Figure 3a) and that of ReB_3 (Figure 3b), consistent with the rich vibrational structures observed experimentally

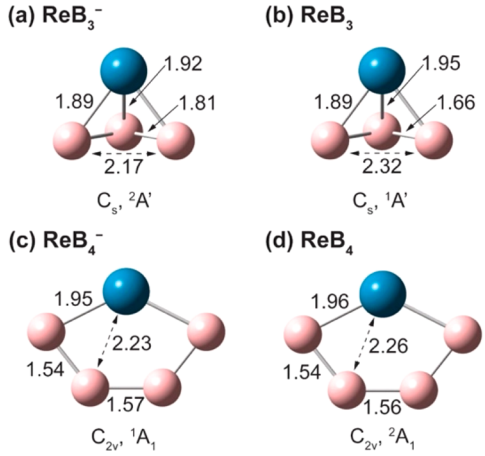

Figure 3. Global minima of (a) ReB_3^-, (b) ReB_3, (c) ReB_4^-, and (d) ReB_4 calculated at the B3LYP/aug-cc-pVTZ/Re/aug-cc-pVTZ-pp level of theory. The bond lengths are in Å.

The SOMO of ReB_3^- (Figure S4a) involves weak bonding interactions between the two terminal B-atoms and antibonding interactions between the terminal B-atoms and the central B-atom. The structure changes are consistent with the bonding characters of the SOMO. The calculated ADE for ReB_3^- is 2.15 eV, in good agreement with the experimental value of 2.1600 eV (Table S1). The vibrational assignments in Table S1 and Figure S2 are assisted by the computed vibrational frequencies (Figure S5a). The vibrational displacement vectors of the two most Franck−Condon-active modes (ν_3 and ν_4) agree with the geometry changes.

The theoretical results show that the structures of ReB_4 and ReB_4^- (Figure 3) are almost identical, consistent with the nonbonding nature of the HOMO of ReB_4^- (Figure S4b) and the simple PE spectra (Figure 2). The calculated EA for ReB_4 is 2.54 eV, agreeing well with the experimental value of 2.5842 eV (Table S2). The weak vibrational features observed in the PE spectra can all be assigned using the computed vibrational frequencies (Table S2). Fundamental excitations in all the symmetric modes (Figure S5b) are observed, and the computed vibrational frequencies agree well with the experimental values. Overall, the excellent agreement between the experimental and theoretical data provides unequivocal evidence for the global minima identified for these metal-laboron clusters.

Several metal triboride clusters (MB_3^-) were investigated previously, and they were found to have different structures.[33,40−42] The role of the M−B-bonding strength determines the structures of metallaboron clusters. For example, TaB_3^- was found to have a planar fan structure, whereas in AuB_3^-, the Au-atom forms a strong σ-bond with one B-atom on a B_3-triangle,[42] akin to a H−B-bond.[43] IrB_3^- was shown to consist of two nearly degenerate structures, both involving an Ir-atom coordinated by an aromatic B_3 unit, one in η^2-fashion (C_{2v}) and another in η^3-fashion (C_{3v}).[40] The structures and bonding of $ReB_3^{-/0}$ are in between those of $TaB_3^{-/0}$ and $IrB_3^{-/0}$. We also analyzed the bonding in the neutral ReB_3 using adaptive natural density partitioning (AdNDP) (Figure 4a).[44] We found three 2c−2e Re−B-bonds, three 3c−2e σ-bonds, one 4c−2e σ-bond, and one 4c−2e π-bond. Although the structure of ReB_3^- displays some

https://dx.doi.org/10.1021/jacs.9b13417
J. Am. Chem. Soc. 2020, 142, 3356−3360

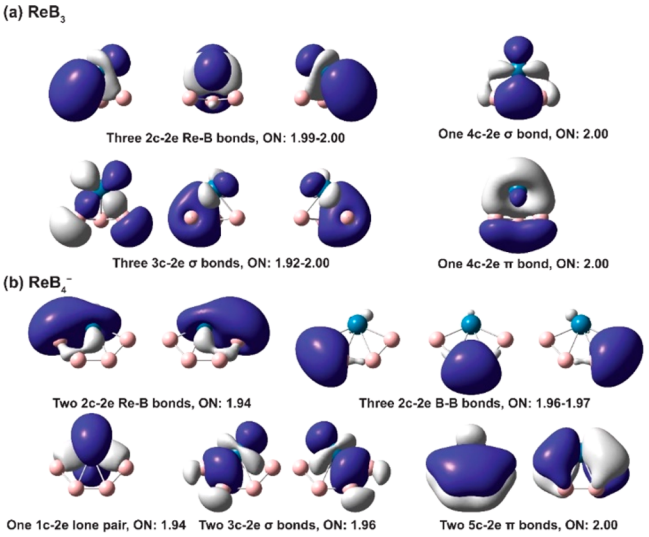

Figure 4. AdNDP analyses of (a) ReB_3 and (b) ReB_4^-.

similarity to the pyramidal structure of IrB_3, their chemical bonding patterns are different. Unlike in IrB_3, all the 5d-electrons of Re involve in bonding with the B-atoms.

Two metal-tetraboride clusters (MB_4^-) were reported previously.[33,41] PrB_4^- was shown to be planar, in which the Pr-atom coordinates to two B-atoms of a rhombus B_4 unit.[41] The structure of TaB_4^- was found to be similar to that of ReB_4^-.[33] In $ReB_4^{-/0}$, the distances between Re- and the B-atoms at the opposite side (2.23 to 2.26 Å) are significantly larger than the Re−B single bond length (2.16 Å) according to Pyykko's atomic radii,[45] suggesting that the structures of $ReB_4^{-/0}$ can be better viewed as pentagonal rings or metallaborocycles.

The AdNDP bonding patterns for ReB_4^- (Figure 4b) are consistent with the pentagonal ring structure, revealing two 2c−2e Re−B σ-bonds and three 2c−2e B−B σ-bonds around the periphery. In addition, there are two 3c−2e σ-bonds between two B-atoms and Re and two 5c−2e delocalized π-bonds. Finally, there is one 1c−2e Re lone pair, mainly of Re $5d_{z2}$ character. It should be pointed out that the previous AdNDP analyses for TaB_4^- localized the two π-MOs into two 3c−2e bonds.[33] For complex systems, solutions of AdNDP analyses are not unique;[44] the solution that best represents the underlying structure is usually chosen. Similar 3c−2e localization can also be done for ReB_4^-, but the 5e−2e solution is a more suitable representation of the bonding situation. Natural population analyses (Figure S6) show that all five atoms in ReB_4^- are involved in bonding.

The presence of the two delocalized π-MOs with four π-electrons in ReB_4^- suggests an antiaromatic system according to the $4n + 2$ Hückel rule. However, its pentagonal structure with almost equal B−B-bonds is consistent with aromatic character. We computed the NICS values for $ReB_4^{-/0}$ to examine the magnetic shielding effects of the delocalized electrons (Table 1). There are different NICS indexes; the $NICS_{zz}$ values are used here, because $NICS(0)_{\pi zz}$ has been deemed to be "the method of choice for NICS evaluation of π-aromaticity of planar rings".[46] It is known that the presence of a heavy atom, such as Re, in a planar ring can introduce a strong local magnetic response, including core contributions that are not related to aromaticity.[47] The heavy atom effects can be seen in the large magnitudes of the $NICS(0)_{zz}$ and $NICS(1)_{zz}$ values for $ReB_4^{-/0}$. The $NICS(0)_{\pi zz}$ index that best represents π-aromaticity in ReB_4^- indicates that it is as aromatic as benzene (Table 1). Because the NICS(0) values contain contributions from σ-aromaticity, we also computed $NICS(1)_{\pi zz}$ (Table S3).[48] We found that the $NICS(1)_{\pi zz}$ (−25.48 ppm) of ReB_4^- is similar to that of benzene (−26.57 ppm). Closer examination of the two π-MOs in $ReB_4^{-/0}$ reveals that one of the π-MOs has a Hückel topology, while the other one has a Möbius topology (Figure S6). Thus, the $ReB_4^{-/0}$ clusters must be Möbius aromatic, according to the $4n$ rule. We further computed the orbital contributions to the π-aromaticity for the closed-shell ReB_4^- (Table 1). The Hückel-type MO (HOMO−5) contributes −9.33 ppm to the $NICS(0)_{\pi zz}$ value, while the Möbius-type MO (HOMO−2) contributes −22.90 ppm. The $NICS(1)_{\pi zz}$ values also show that the Möbius MO contributes more to the π-aromaticity (Table S3).

Both TaB_4^- and TaB_5^- were found previously to be planar cyclic systems with two π-MOs including one with Möbius topology (Figure S7).[33] The MOs of TaB_4^- are similar to those of ReB_4^-, except that the latter contains a nonbonding MO of Re $5d_z2$ character (Figure S4b). We also computed the $NICS_{zz}$ values for TaB_4^- and TaB_5^- (Tables 1 and S3). Their negative NICS values imply that both TaB_4^- and TaB_5^- are also Möbius aromatic with 4 π-electrons. A compound $[(OC)_2Fe(BN(SiMe_3)_2)(BDur)]_2$ (**1**) reported previously was shown to contain a central FeB_4 unit with similar atomic connectivity as that in ReB_4^- and TaB_4^-.[49] However, the bonding situation in **1** is different from that in the latter. In **1**, each B-atom undergoes sp^2 hybridization forming a single B−B or B−Fe σ-bond with the neighboring B- or Fe-atom. Each B-atom also forms a σ-bond with a ligand (B−C-bond for the Dur ligand or B−N-bond for the $N(SiMe_3)_2$ ligand), whereas the Fe-atom is coordinated by two CO ligands. The B−B-bond lengths in **1** are quite long (1.729−1.818 Å), where the two B−B-bonds near the Fe-atom also engage in σ-donation to Fe and back-donation from the Fe $3d_z2$ orbital.[49]

In conclusion, we report an experimental and computational study of two redoped boron clusters, ReB_3^- and ReB_4^-. While

Table 1. Comparisons of the NICS Values (in ppm) of $ReB_4^{-/0}$, TaB_4^-, and TaB_5 with Those of Benzene at the B3LYP/SDD Level of Theory

	$NICS(0)_{zz}$	$NICS(1)_{zz}$	$NICS(0)_{\pi zz}$	$NICS(0)_{Hückel,zz}$	$NICS(0)_{Möbius,zz}$
C_6H_6	−3.16	−24.95	−31.71		
ReB_4^-	−144.11	−52.10	−32.23	−9.33	−22.90
ReB_4	−132.87	−54.12	*a*	*a*	*a*
TaB_4^-	−126.25	−58.18	−32.23	−10.63	−21.60
TaB_5	−29.67	−28.34	−28.38	−10.37	−18.01

[a]Natural chemical shielding analysis for open-shell systems is not available.

https://dx.doi.org/10.1021/jacs.9b13417
J. Am. Chem. Soc. 2020, 142, 3356−3360

ReB_3^- is found to have a near-pyramidal structure, ReB_4^- is observed to be a planar pentagonal ring. ReB_4^- is found to possess two delocalized π-MOs, one of which has a Möbius topology. Computed NICS values and comparison with those of benzene reveal that $ReB_4^{-/0}$ is aromatic and the first Möbius aromatic metallaborocycle. We expect that there may exist a new class of Möbius aromatic metallaborons.

■ ASSOCIATED CONTENT

Supporting Information

The Supporting Information is available free of charge at https://pubs.acs.org/doi/10.1021/jacs.9b13417.

Detailed description of the experimental and computational methods, full experimental data set for ReB_3^-, computed vibrational frequencies and molecular orbitals of ReB_3^- and ReB_4^-, molecular orbitals of TaB_4^- and TaB_5^-, detailed experimental results of ReB_3^- and ReB_4^-, atomic orbital contribution for the π-orbitals of ReB_4^-, and optimized Cartesian coordinates for the global minima of $ReB_3^{-/0}$ and $ReB_4^{-/0}$ (PDF)

■ AUTHOR INFORMATION

Corresponding Author

Lai-Sheng Wang − *Department of Chemistry, Brown University, Providence, Rhode Island 02912, United States;* orcid.org/0000-0003-1816-5738; Email: lai-sheng_wang@brown.edu

Authors

Ling Fung Cheung − *Department of Chemistry, Brown University, Providence, Rhode Island 02912, United States;* orcid.org/0000-0002-2308-8135

G. Stephen Kocheril − *Department of Chemistry, Brown University, Providence, Rhode Island 02912, United States;* orcid.org/0000-0003-1388-6472

Joseph Czekner − *Department of Chemistry, Brown University, Providence, Rhode Island 02912, United States*

Complete contact information is available at: https://pubs.acs.org/10.1021/jacs.9b13417

Notes

The authors declare no competing financial interest.

■ ACKNOWLEDGMENTS

This work was supported by the National Science Foundation (Grant CHE-1763380).

■ REFERENCES

(1) Heilbronner, E. Hückel Molecular Orbitals of Möbius-Type Conformations of Annulenes. *Tetrahedron Lett.* **1964**, *5*, 1923−1928.

(2) Rzepa, H. S. Möbius Aromaticity and Delocalization. *Chem. Rev.* **2005**, *105*, 3697−3715.

(3) Ajami, D.; Oeckler, O.; Simon, A.; Herges, R. Synthesis of a Möbius Aromatic Hydrocarbon. *Nature* **2003**, *426*, 819−821.

(4) Craig, D. P.; Paddock, N. L. A Novel Type of Aromaticity. *Nature* **1958**, *181*, 1052−1053.

(5) Kos, A. J.; Schleyer, P. v. R. Cyclic 4π Stabilization. Combined Möbius-Hückel Aromaticity in Doubly Lithium Bridged $R_4C_4Li_2$ Systems. *J. Am. Chem. Soc.* **1980**, *102*, 7928−7929.

(6) Fernández, I.; Frenking, G. Aromaticity in Metallabenzenes. *Chem. - Eur. J.* **2007**, *13*, 5873−5884.

(7) Fernández, I.; Frenking, G.; Merino, G. Aromaticity of Metallabenzenes and Related Compounds. *Chem. Soc. Rev.* **2015**, *44*, 6452−6463.

(8) Mauksch, M.; Tsogoeva, S. B. Demonstration of "Möbius" Aromaticity in Planar Metallacycles. *Chem. - Eur. J.* **2010**, *16*, 7843−7851.

(9) Zhu, C.; Li, S.; Luo, M.; Zhou, X.; Niu, Y.; Lin, M.; Zhu, J.; Cao, Z.; Lu, X.; Wen, T.; Xie, Z.; Schleyer, P. v. R.; Xia, H. Stabilization of Anti-aromatic and Strained Five-Membered Rings with a Transition Metal. *Nat. Chem.* **2013**, *5*, 698−703.

(10) Zhu, C.; Luo, M.; Zhu, Q.; Zhu, J.; Schleyer, P. v. R.; Wu, J. I. C.; Lu, X.; Xia, H. Planar Möbius Aromatic Pentalenes Incorporating 16 and 18 Valence Electron Osmiums. *Nat. Commun.* **2014**, *5*, 3265.

(11) Wei, J.; Zhang, Y.; Chi, Y.; Liu, L.; Zhang, W. X.; Xi, Z. F. Aromatic Dicupra[10]annulenes. *J. Am. Chem. Soc.* **2016**, *138*, 60−63.

(12) An, K.; Shen, T.; Zhu, J. Craig-Type Möbius Aromaticity and Antiaromaticity in Dimetalla[10]annulenes: A Metal-Induced Yin-and-Yang Pair. *Organometallics* **2017**, *36*, 3199−3204.

(13) Frogley, B. J.; Wright, L. J. Recent Advances in Metallaaromatic Chemistry. *Chem. - Eur. J.* **2018**, *24*, 2025−2038.

(14) Mauksch, M.; Tsogoeva, S. B. Strict Correlation of HOMO Topology and Magnetic Aromaticity Indices in d-Block Metalloaromatics. *Chem. - Eur. J.* **2018**, *24*, 10059−10063.

(15) Chen, D.; Xie, Q.; Zhu, J. Unconventional Aromaticity in Organometallics: The Power of Transition Metals. *Acc. Chem. Res.* **2019**, *52*, 1449−1460.

(16) Mauksch, M.; Tsogoeva, S. B. Hückel and Möbius Aromaticity in Charged Sigma Complexes. *Chem. - Eur. J.* **2019**, *25*, 7457−7462.

(17) Szczepanik, D. W.; Solà, M. Electron Delocalization in Planar Metallacycles: Hückel or Möbius Aromatic? *ChemistryOpen* **2019**, *8*, 219−227.

(18) Alexandrova, A. N.; Boldyrev, A. I.; Zhai, H. J.; Wang, L. S. All-boron Aromatic Clusters as Potential New Inorganic Ligands and Building Blocks in Chemistry. *Coord. Chem. Rev.* **2006**, *250*, 2811−2866.

(19) Sergeeva, A. P.; Popov, I. A.; Piazza, Z. A.; Li, W. L.; Romanescu, C.; Wang, L. S.; Boldyrev, A. I. Understanding Boron through Size-Selected Clusters: Structure, Chemical Bonding, and Fluxionality. *Acc. Chem. Res.* **2014**, *47*, 1349−1358.

(20) Wang, L. S. Photoelectron Spectroscopy of Size-selected Boron Clusters: from Planar Structures to Borophenes and Borospherenes. *Int. Rev. Phys. Chem.* **2016**, *35*, 69−142.

(21) Zhai, H. J.; Kiran, B.; Li, J.; Wang, L. S. Hydrocarbon Analogues of Boron Clusters—Planarity, Aromaticity and Antiaromaticity. *Nat. Mater.* **2003**, *2*, 827−833.

(22) Zhai, H. J.; Alexandrova, A. N.; Birch, K. A.; Boldyrev, A. I.; Wang, L. S. Hepta- and Octacoordinate Boron in Molecular Wheels of Eight- and Nine-Atom Boron Clusters: Observation and Confirmation. *Angew. Chem., Int. Ed.* **2003**, *42*, 6004−6008.

(23) Sergeeva, A. P.; Zubarev, D. Y.; Zhai, H. J.; Boldyrev, A. I.; Wang, L. S. A Photoelectron Spectroscopic and Theoretical Study of B_{16}^- and B_{16}^{2-}: An All-Boron Naphthalene. *J. Am. Chem. Soc.* **2008**, *130*, 7244−7246.

(24) Huang, W.; Sergeeva, A. P.; Zhai, H. J.; Averkiev, B. B.; Wang, L. S.; Boldyrev, A. I. A Concentric Planar Doubly π-Aromatic B_{19}^- Cluster. *Nat. Chem.* **2010**, *2*, 202−206.

(25) Sergeeva, A. P.; Piazza, Z. A.; Romanescu, C.; Li, W. L.; Boldyrev, A. I.; Wang, L. S. B_{22}^- and B_{23}^-: All-Boron Analogues of Anthracene and Phenanthrene. *J. Am. Chem. Soc.* **2012**, *134*, 18065−18073.

(26) Piazza, Z. A.; Hu, H. S.; Li, W. L.; Zhao, Y. F.; Li, J.; Wang, L. S. Planar Hexagonal B_{36} as a Potential Basis for Extended Single-Atom Layer Boron Sheets. *Nat. Commun.* **2014**, *5*, 3113.

(27) Boldyrev, A. I.; Wang, L. S. Beyond Organic Chemistry: Aromaticity in Atomic Clusters. *Phys. Chem. Chem. Phys.* **2016**, *18*, 11589−11605.

(28) Pan, S.; Barroso, J.; Jalife, S.; Heine, T.; Asmis, K. R.; Merino, G. Fluxional Boron Clusters: From Theory to Reality. *Acc. Chem. Res.* **2019**, *52*, 2732−2744.

(29) Cheung, L. F.; Czekner, J.; Kocheril, G. S.; Wang, L. S. ReB_6^-: A Metallaboron Analog of Metallabenzenes. *J. Am. Chem. Soc.* **2019**, *141*, 17854−17860.

(30) Romanescu, C.; Galeev, T. R.; Li, W. L.; Boldyrev, A. I.; Wang, L. S. Aromatic Metal-Centered Monocyclic Boron Rings: $Co©B_8^-$ and $Ru©B_9^-$. *Angew. Chem., Int. Ed.* **2011**, *50*, 9334−9337.
(31) Li, W. L.; Romanescu, C.; Galeev, T. R.; Piazza, Z. A.; Boldyrev, A. I.; Wang, L. S. Transition-Metal-Centered Nine-Membered Boron Rings: $M©B_9$ and $M©B_9^-$ (M = Rh, Ir). *J. Am. Chem. Soc.* **2012**, *134*, 165−168.
(32) Romanescu, C.; Galeev, T. R.; Li, W. L.; Boldyrev, A. I.; Wang, L. S. Transition-Metal-Centered Monocyclic Boron Wheel Clusters ($M©B_n$): A New Class of Aromatic Borometallic Compounds. *Acc. Chem. Res.* **2013**, *46*, 350−358.
(33) Li, W. L.; Ivanov, A. S.; Federič, J.; Romanescu, C.; Černušák, I.; Boldyrev, A. I.; Wang, L. S. On the Way to The Highest Coordination Number in the Planar Metal-Centred Aromatic $Ta©B_{10}^-$ Cluster: Evolution of the Structures of TaB_n^- (n = 3−8). *J. Chem. Phys.* **2013**, *139*, 104312.
(34) Chen, T. T.; Li, W. L.; Bai, H.; Chen, W. J.; Dong, X. R.; Li, J.; Wang, L. S. $Re©B_8^-$ and $Re©B_9^-$: New Members of the Transition-Metal-Centered Borometallic Molecular Wheel Family. *J. Phys. Chem. A* **2019**, *123*, 5317−5324.
(35) Popov, I. A.; Li, W. L.; Piazza, Z. A.; Boldyrev, A. I.; Wang, L. S. Complexes between Planar Boron Clusters and Transition Metals: A Photoelectron Spectroscopy and Ab Initio Study of CoB_{12}^- and RhB_{12}. *J. Phys. Chem. A* **2014**, *118*, 8098−8105.
(36) Schleyer, P. v. R.; Maerker, C.; Dransfeld, A.; Jiao, H.; van Eikema Hommes, N. J. R. Nucleus-Independent Chemical Shifts: A Simple and Efficient Aromaticity Probe. *J. Am. Chem. Soc.* **1996**, *118*, 6317−6318.
(37) León, I.; Yang, Z.; Liu, H. T.; Wang, L. S. The Design and Construction of a High-Resolution Velocity-Map Imaging Apparatus for Photoelectron Spectroscopy Studies of Size-Selected Clusters. *Rev. Sci. Instrum.* **2014**, *85*, No. 083106.
(38) Becke, A. D. Density-Functional Thermochemistry. III. The Role of Exact Exchange. *J. Chem. Phys.* **1993**, *98*, 5648−5652.
(39) Watts, J. D.; Gauss, J.; Bartlett, R. J. Coupled-Cluster Methods with Noniterative Triple Excitations for Restricted Open-Shell Hartree−Fock and Other General Single Determinant Reference Functions. Energies and Analytical Gradients. *J. Chem. Phys.* **1993**, *98*, 8718−8733.
(40) Czekner, J.; Cheung, L. F.; Kocheril, G. S.; Kulichenko, M.; Boldyrev, A. I.; Wang, L. S. High-Resolution Photoelectron Imaging of IrB_3^-: Observation of a π-Aromatic B_3^+ Ring Coordinated to a Transition Metal. *Angew. Chem., Int. Ed.* **2019**, *58*, 8877−8881.
(41) Chen, X.; Chen, T. T.; Li, W. L.; Lu, J. B.; Zhao, L. J.; Jian, T.; Hu, H. S.; Wang, L. S.; Li, J. Lanthanide with Unusually Low Oxidation States in the PrB_3^- and PrB_4^- Boride Clusters. *Inorg. Chem.* **2019**, *58*, 411−418.
(42) Chen, Q.; Bai, H.; Zhai, H. J.; Li, S. D.; Wang, L. S. Photoelectron spectroscopy of boron-gold alloy clusters and boron boronyl clusters: $B_3Au_n^-$ and $B_3(BO)_n^-$ (n = 1, 2). *J. Chem. Phys.* **2013**, *139*, No. 044308.
(43) Wang, L. S. Covalent Gold. *Phys. Chem. Chem. Phys.* **2010**, *12*, 8694−8705.
(44) Zubarev, D. M.; Boldyrev, A. I. Developing Paradigms of Chemical Bonding: Adaptive Natural Density Partitioning. *Phys. Chem. Chem. Phys.* **2008**, *10*, 5207−5217.
(45) Pyykkö, P. Additive Covalent Radii for Single-, Double-, and Triple-Bonded Molecules and Tetrahedrally Bonded Crystals: A Summary. *J. Phys. Chem. A* **2015**, *119*, 2326−2337.
(46) Fallah-Bagher-Shaidaei, H.; Wannere, C. S.; Corminboeuf, C.; Puchta, R.; Schleyer, P. v. R. Which NICS Aromaticity Index for Planar π Rings Is Best? *Org. Lett.* **2006**, *8*, 863−866.
(47) Orozco-Ic, M.; Barroso, J.; Charistos, N. D.; Muñoz-Castro, A.; Merino, G. Consiquences of Curvature on Induced Magnetic Field: The Case of Helicenes. *Chem. - Eur. J.* **2020**, *26*, 326−330.
(48) Sun, H.; An, K.; Zhu, J. Triplet State Aromaticity: NICS Criterion, Hyperconjugation, and Charge Effects. *Chem. - Asian J.* **2016**, *11*, 234−240.
(49) Braunschweig, H.; Ye, Q.; Vargas, A.; Dewhurst, R. D.; Radacki, K.; Damme, A. Controlled Homocatenation of Boron on a Transition Metal. *Nat. Chem.* **2012**, *4*, 563−567.

https://dx.doi.org/10.1021/jacs.9b13417
J. Am. Chem. Soc. 2020, 142, 3356−3360